Lab on a Chip

Cite this: *Lab Chip*, 2012, **12**, 5231–5236

www.rsc.org/loc

PAPER

Optical non-contact localization of liquid-gas interfaces on disk during rotation for measuring flow rates and viscosities

Jochen Hoffmann,†[a] Lutz Riegger,†*[a] Frederik Bundgaard,[a] Daniel Mark,[a] Roland Zengerle[abc] and Jens Ducrée[d]

Received 24th July 2012, Accepted 10th October 2012
DOI: 10.1039/c2lc40842b

We present a novel technique for the spatio-temporally resolved localization of liquid-gas interfaces on centrifugal microfluidic platforms based on total internal reflection (TIR) at the channel wall. The simple setup consists of a line laser and a linear image sensor array mounted in a stationary instrument. Apart from identifying the presence of usually unwanted gas bubbles, the here described online meniscus detection allows to measure liquid volumes with a high precision of 1.9%. Additionally, flow rates and viscosities (range: 1–12 mPa s, precision of 4.3%) can be sensed even during rotation at frequencies up to 30 Hz.

Introduction

Lab-on-a-chip systems make specific use of significant shifts in hydrodynamic force ratios towards miniaturized environments.[1] In more detail, surface-to-volume ratios increase, thus letting surface mediated effects such as surface tension and viscous drag prevail over bulk forces such as inertia and gravity.[2,3] Amongst the most cited consequences are the establishment of strictly laminar flow conditions and flow control through "active channel" mechanisms such as capillarity and electroosmosis.

Lab-on-a-chip devices typically concatenate laboratory unit operations for liquid handling such as sample preparation, aliquoting, metering, and mixing on a single substrate[4,5] to perform bio-chemical assays in a process-integrated, automated, miniaturized and often parallel fashion.[6] However, due to their strong dependency on often hard to control surface properties, lab-on-a-chip systems are intrinsically prone to inconsistencies such as the formation of gas bubbles or pockets during priming and operation.[7,8] This tendency may lead to insufficient filling of microfluidic cavities with sample or reagents. In flow cytometry, droplet-based systems, or lateral flow assays, functionality is critically dependent on the precise definition of flow rates.[9] In order to leverage a successful transfer of academic lab-on-a-chip technology to real-world applications, it is therefore key to introduce some form of (ideally) closed-loop process control which monitors the course of liquid flow.

A range of different miniaturized flow-rate sensors have been developed which rely on optical beam deflection,[10] heat transfer,[11–14] time-of-flight measurements using tracers,[15,16] pressure differences,[17] or drag-force induced changes in electrical parameters.[18–21] While excellent performance of these sensors has been demonstrated, their application to lab-on-a-chip systems is often burdened by complex sensor architectures, interference with the flow and media, costs, and fabrication issues. For instance the detection of often detrimental trapped air bubbles has so far been practically implemented either by the bare eye or only retrospectively after the failure of a microfluidic experiment.

To this end, we previously presented a technique based on TIR on the channel wall to localize liquid-gas interfaces in microchannels at rest.[22] In this contribution, we present its implementation on a centrifugal microfluidic platform.[23–28] Our technique is based on linear illumination and detection elements allowing quasi-continuous meniscus detection (*e.g.* the liquid level), even at high spin speeds of rotation up to 30 Hz. Furthermore, the technique allows for accurate and reproducible flow rates and viscosity measurement in centrifugal microfluidic systems.

Materials and methods

Microfluidic disk

The microfluidic design is realized into a disk made of cyclo olefin copolymer (TOPAS COC 5013 disks, microfluidic ChipShop, Jena, Germany) by a micromilling machine (Mini-Mill 3 Pro, Minitech Machinery Corp., Norcross, USA). As depicted in Fig. 1, the disk contains four paired channels exhibiting a triangular cross-section with a wall inclination angle of 45°. Each pair has one measurement channel (Fig. 1, b) and one auxiliary channel which is permanently filled with air (Fig. 1, a). Each pair of channels is laterally shifted by 7.5 mm with

[a]*Laboratory for MEMS Applications, Department of Microsystems Engineering-IMTEK, University of Freiburg, Georges-Koehler-Allee 103, Freiburg, 79110, Germany. E-mail: zengerle@imtek.de; Fax: +49 761 203 73299; Tel: +49 761 203 73213*
[b]*HSG-IMIT, Wilhelm-Schickard-Straße 10, D-78052 Villingen-Schwenningen, Germany*
[c]*BIOSS–Centre for Biological Signalling Studies, University of Freiburg*
[d]*BDI–Biomedical Diagnostics Institute, National Centre for Sensor Research, School of Physical Sciences, Dublin City University, Glasnevin, Dublin 9, Ireland*
† These authors contributed equally to this work.

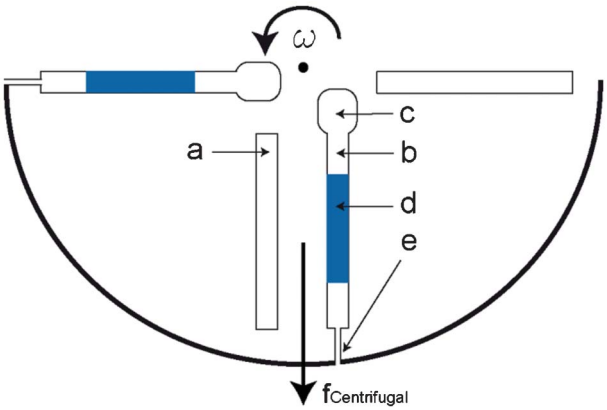

Fig. 1 Schematic drawing of one half of the on-disk structure, showing all relevant channels and geometric features referred to. Legend: a) auxiliary channel; b) measurement channel; c) inlet reservoir; d) liquid plug; e) microchannel.

respect to a central radial line. Channels have a depth of 1.5 mm and a width of 3 mm. The inner end of the measurement channel near the center of rotation is connected to an inlet reservoir. The radially outer side of the channel leads to a rectangular flow restriction channel measuring 400 μm in width, 100 μm in depth, and 4 mm in length, referred to as microchannel (Fig. 1, e).

Optical components and read-out

The optical measurement components comprise a line laser and a linear image sensor array. The laser diode emits at the peak-wavelength λ_{peak} = 650 nm and possesses a maximum optical power of 24 mW (RLLH650-24-3, Roithner, Roithner Lasertechnik GmbH, Vienna, Austria). The housing contains this diode as well as a special optic generating the probe line. The CMOS linear image sensor (S8377-512Q, Hamamatsu, Herrsching am Ammersee, Germany) used is a compact sensor featuring a built-in timing generator as well as a signal processing circuit. The active area amounts to 25.6 × 0.5 mm subdivided into 512 individual pixels (resulting in a pixel pitch of 50 μm and a pixel height of 500 μm).

An electrical controlling unit (OEM Electronics for Linear arrays, Spectronics Devices Ltd., Bedford, United Kingdom) is used to address the operating mode of the sensor as well as to transfer optical data to a PC. The set comprises two small-size printed circuit boards (PCB): a 50 mm × 20 mm PCB holding the sensor incorporating pre-amplifier and A/D converter electronics and a second PCB with the control electronics, a 1 MByte data storage memory for saving 1000 scans and a USB PC interface. The processing time for one scan takes only 2 μs, which allows the required high-speed data acquisition.

Experimental setup

The setup is shown in Fig. 2. It consists of a device (player)[29] which spins the disk-shaped lab-on-a-chip substrates at well-defined rotational frequencies and acceleration rates. The measurement components, *i.e.* line laser (Fig. 2, a), linear image sensor (Fig. 2, b), and one electrical control unit (Fig. 2, c) are assembled on a PMMA plate and positioned perpendicularly above the disk.

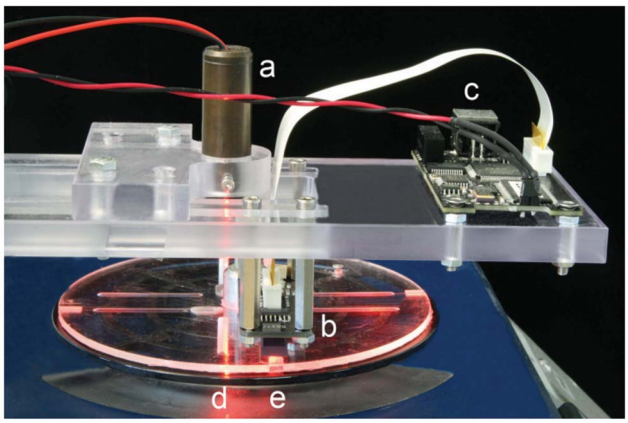

Fig. 2 Photo of the experimental setup. The beam is issued from a line laser onto the rotating substrate and reflected back to a linear image sensor. Legend: a) line laser; b) linear image sensor; c) electrical controlling unit; d) auxiliary channel; e) measurement channel.

Functional principle

According to Snell's law, TIR at an interface occurs when the ratio of refractive indices of the bulk material of the disc (n_{COC} = 1.49) and the medium inside the channel exceeds 1.41.

A laser beam which impinges on the 45° inclination of the wall of the auxiliary channel (Fig. 3, d) is thus deflected by a total 90° into the plane of the substrate. Next, the beam impinges on the inclined wall of the measurement channel (Fig. 3, e). If a segment of this channel is filled with air, a second TIR redirects the laser beam by 90° towards the linear image sensor (Fig. 3, b). If segments are filled by liquid, a change in local refractive indices occurs and rules out TIR (n >1.06). As a result, the beam fails to impinge on the sensor as the beam simply traverses the disk.

The emitting power of the line laser is set to a value of 5 mW which is sufficient for saturating those pixels receiving the signal. Thereby, a discrete, binary signal is obtained where 1 indicates

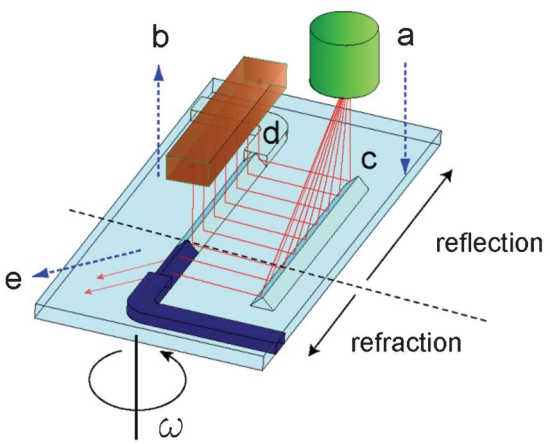

Fig. 3 Illustration of the liquid-air interface detection. The laser beam is emitted perpendicular to the disk surface (a). When the auxiliary channel (c) and the measurement channel (d) are filled with air, total internal reflection occurs, redirecting the beam twice back towards the sensor (b). When a channel segment is filled with liquid, the laser beam is refracted and guided through the bottom side of the disk (e), where the beam is not accessible to the sensor.

an empty section and 0 a liquid-filled section of the channel. This works up to frequencies of 30 Hz. At higher frequencies, a higher emitting power is required.

The azimuthal position of the channels on the disk and the sensor position are synchronized by using the TTL-signal provided by the player once per revolution as a command-signal for the sensor. The linear image sensor starts to acquire optical data each time the rising flank of the trigger signal is detected and stops after a certain integration time being dependent on the rotational frequency. The length of the integration time is chosen to cover one disk-sector featuring one channel pair for each revolution. Thereby, a consistent and stable measurement system is guaranteed requiring no alignment or signal strength calibration. This measurement principle is applied for all dynamic measurements like flow rate sensing and viscosity measurements.

Each combination of measurement channel and microchannel represents a hydrodynamic resistance as in eqn (1).

$$R_{hd} = R_{hd,measure} + R_{hd,micro} \quad (1)$$

For laminar flow conditions, the hydrodynamic resistance R_{hd} of rectangular cross sections (*i.e.*, the microchannel) can be expressed as in eqn (2)[30] (η: dynamic viscosity, l: channel length, h: channel height, w: channel width).

$$R_{hd} = \frac{8\eta l}{\rho} \frac{\left(1 + \frac{h}{w}\right)^2}{wh^3} \quad (2)$$

The geometry of the channels is chosen so that the resistance of the outlet microchannel exceeds the resistance of the measurement channel by four orders of magnitude. Thus, we will calculate the total flow resistance R_{hd} by considering the geometry of the outlet channel only. By only measuring the liquid level in the measurement channel, the hydrodynamic resistance can therefore be considered constant for liquids with equal viscosities.

Experimental results

The power of the new measurement technique is evaluated in terms of bubble detection, flow rate, and viscosity measurements. All measurements are performed at 22 °C in an air-conditioned laboratory.

Bubble detection

A representative plot for the pixel intensity along a measurement channel entrapping an air bubble under static conditions is shown in Fig. 4, revealing clearly discernible flanks at the respective liquid-gas interfaces. Using proper curve fitting algorithms, the position of the meniscus can be pinpointed down to roughly 3 pixels, corresponding to a radial resolution of 150 μm.

Volume calibration

For a given microchannel geometry, the theoretical maximum filling level is calculated with respect to the length of the channel. In the next step, the active area of the linear image sensor is laterally shifted (positioned) in such a way that it provides output characteristics corresponding to the calculated liquid level. Once the system is calibrated, the measurements described in the following sections are performed. For the volume calibration, liquid-levels of the five different volumes 10 μL, 15 μL, 20 μL, 25 μL and 30 μL are measured five times each. Each measurement is conducted under rotation at 10 Hz whereby the position of the liquid-gas interface is averaged over 10 revolutions with one measurement per revolution. Fig. 5 displays a calibration curve with five pre-metered volumes, featuring a high accuracy and a precision of 1.9%.

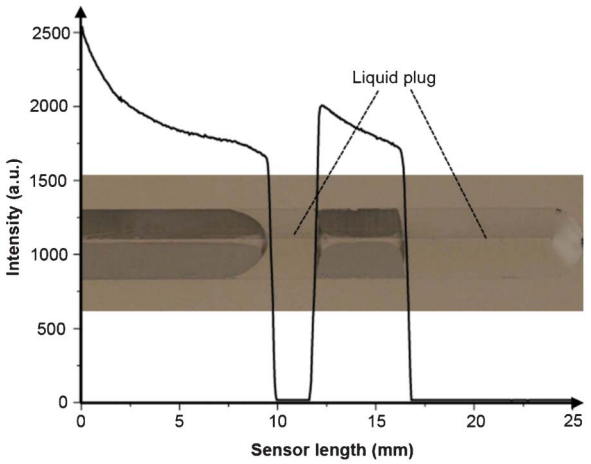

Fig. 4 Measured pixel intensity plot of a bubble within a channel captured by the linear image sensor at rest. The transition between liquid and gas state is very distinct thus allowing a clear localization of the meniscus.

Flow rate and viscosity measurement

A comprehensive overview over advances in rheological measurement techniques is presented by Hou *et al.*[31] Quist *et al.* presented a MEMS-based systems for accurately measuring viscosities under laminar flow conditions.[21] Czaplewski *et al.* measured viscosities in microchannels by measuring the viscosity-dependent deflection of an optical beam.[10] Nevertheless, both

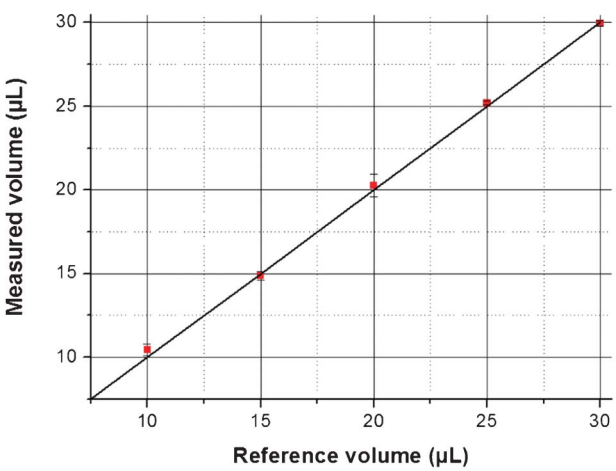

Fig. 5 Calibration of measured volumes with pre-metered volumes.

sensors are invasive to the liquid flow, complex in architecture, and expensive in fabrication.

In centrifugal systems, the time dependent volumetric flow rate I_v can be expressed as in eqn (3)[30] (V: liquid volume, A: channel cross section, $r_<$: inner radial meniscus position, $r_>$: outer radial meniscus position, Δp_ω: centrifugal pressure, ρ: fluid density, ω: rotational frequency).

$$I_v(t) = \frac{dV(t)}{dt} = \frac{dAr_<(t)}{dt} = \frac{\Delta p_\omega}{R_{hd}} = \frac{\rho\omega^2}{2R_{hd}}\left(r_>^2 - r_<(t)^2\right) \quad (3)$$

Consequently, the flow rate can be measured by monitoring the inner radial meniscus position for a liquid with constant outer meniscus $r_>$ "pinned" at the exit and known density ρ and viscosity η. The latter can be determined in the following way. First, the time derivative of the liquid level is expressed as in eqn (4) and eqn (5):

$$\frac{dr_<(t)}{dt} = \frac{\rho\omega^2}{2AR_{hd}}\left(r_>^2 - r_<(t)^2\right) \quad (4)$$

$$\frac{dr_<(t)}{\left(r_>^2 - r_<(t)^2\right)} = \frac{\rho\omega^2}{2AR_{hd}}dt \quad (5)$$

Integrating leads to the following equations for the liquid level (C = integral constant, k = fit variable) as in eqn (6) and eqn (7):

$$\frac{\tanh^{-1}\left(\frac{r_<(t)}{r_>}\right)}{r_>} = \frac{\rho\omega^2}{2AR_{hd}}t + C \quad (6)$$

$$r_<(t) = r_>\tanh\left(\frac{r_>\rho\omega^2}{2AR_{hd}}t + C\right) = r_>\tanh(kt + C) \quad (7)$$

Finally, the dynamic viscosity is derived as in eqn (8):

$$\eta = \frac{r_>\rho\omega^2 wh^3}{16Al\left(1 + \frac{h}{w}\right)^2}\frac{t}{\left(\tanh^{-1}\left(\frac{r_<(t)}{r_>}\right) - C\right)} \quad (8)$$

Due to the strong dependence of the viscosity on the channel dimensions (which are prone to vary, especially in milled structures), the same channel is used for referencing as well as measurement in this approach. Thus, the unknown viscosity is determined with eqn (9):

$$\eta_{measure} = \frac{k_{reference}\rho_{measure}}{k_{measure}\rho_{reference}}\eta_{reference} \quad (9)$$

The k values can be determined by fitting viscosity measurement data based on the denoted equation. Measurement data is acquired by centrifugally driven discharge induced *via* constant rotational frequency of 10 Hz or 20 Hz for more viscous (η >5 mPa s) liquids. Tests are based on four different glycerol solutions with dynamic viscosities in the range of 1.0–12.0 mPa s, *i.e.* 1.2 mPa s, 2.0 mPa s, 5.7 mPa s, and 12.0 mPa s. 25 μL of each sample liquid is pipetted into the inlet reservoir. Fluids are driven through the measurement channel by centrifugal forces and pass the adjoining microchannel while the liquid level is constantly monitored. Each viscosity is measured five times. To demonstrate the capability for flow rate measurement, a representative value is selected from each viscosity set to calculate the respective flow rate.

For the investigated samples of different viscosity η, exemplary flow rate measurements are depicted in Fig. 6. The data reveals the $1/\eta$ dependency for the initial flow rate as well as the non-linear decrease due to dynamically decreasing liquid level. Contact-free and on-line determination of the flow rate provides an insight into liquid guidance on lab-on-a-disk systems. Furthermore, the implementation of a feedback-loop can improve the liquid guidance on-disk and contribute to a better controllable fluidic system.

Fig. 7 demonstrates the capability of the system to measure the dynamic viscosity of low-viscous liquids which is verified by the good agreement between the calculated curves and the measured data.

The previously described glycerol solutions are used to highlight the correlation between the measured viscosities and the reference viscosities as shown in Fig. 8. Here, a mean precision of 4.3% is achieved.

Summary and conclusion

This work introduces a novel TIR-based setup with optical elements for spatio-temporally resolved meniscus detection on a rotating microfluidic platform. The performance of this measurement system is investigated in the context of bubble detection in microchannels, as well as the measurement of liquid levels, flow-rates, and viscosities.

The liquid-gas interface in a microchannel is optically pinpointed down to 150 μm whereby a probing laser beam is either reflected (in the presence of air) or refracted (in the presence of liquid). By this TIR principle, we measured flow rates from 0.5 μL s^{-1} to 7.7 μL s^{-1} and viscosities in the low regime from 1.0–12.0 mPa s with a precision of 4.3%. The

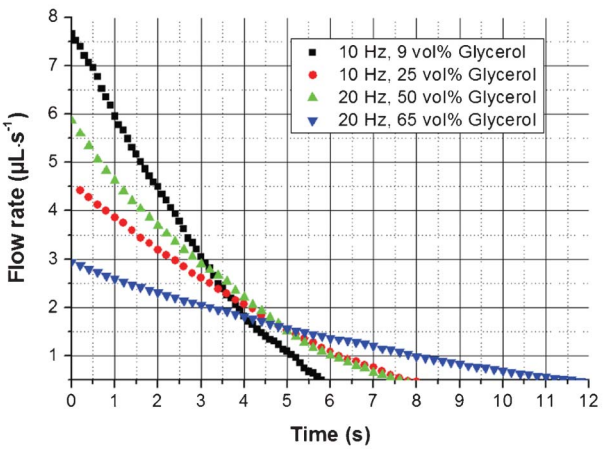

Fig. 6 Flow rate measurement derived from a time-resolved liquid-level determination with the calibrated system, utilizing two different rotational frequencies. The relative decrease of the flow rate correlates with increasing viscosity.

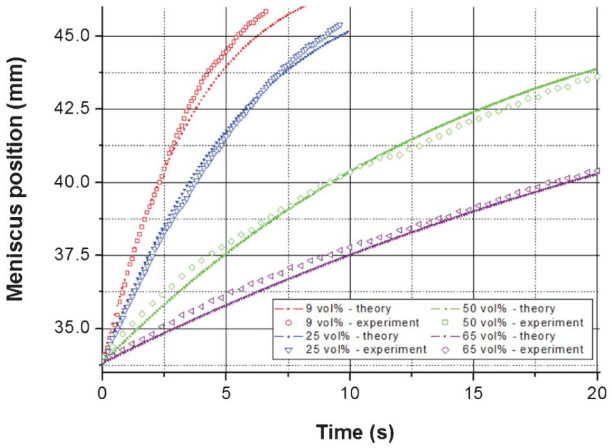

Fig. 7 Calculated and measured liquid level progression for glycerol samples featuring different viscosities. The respective curves are in good agreement.

unprecedented dynamic recordings of flow rates and viscosities during rotation are enabled by a line laser and linear image sensor in contrast to the static scanning principle of our previous work.[22] The spatial resolution could be further increased by using a linear image sensor featuring a pixel pitch <50 μm. This would improve the measuring precision because the meniscus could be pinpointed more accurately. Compared to other methods for viscosity measurements, our system excels with low sample consumption, a simple, low-cost setup of the measurement instrument, and the option to reuse a potentially precious sample after measurement from a reservoir. Currently, only Newtonian liquids have been investigated. As the system is capable of measuring the time-dependent and, in this case, shear-dependent viscosity by means of the flow rate, the viscosity of non-Newtonian liquids could also be determined. Here, the shear and thus time-dependent viscosity would be calculated directly (*i.e.*, without curve fitting) by resorting to the Weissenberg–Rabinowitsch–Mooney correction.[32]

Despite excellent performance of published flow rate sensors in terms of sensitivity and measurement ranges,[9–21] some appear intrinsically inadequate for a smart integration into lab-on-a-chip systems. In contrast, our system excels with compact, low cost components and its non-contact and non-invasive measurement principle. No pre-treatment of the fluid is required, as may be the case in time-of-flight measurements introducing particles which may have an impact on the fluidic itself.[15,16]

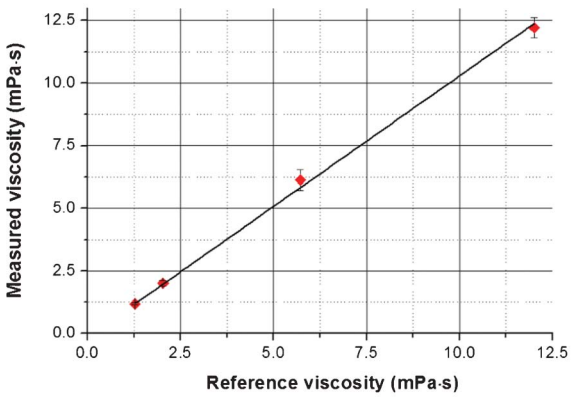

Fig. 8 Dynamic viscosity measurement featuring a reproducibility of 4.3% for viscosities up to 12 mPa s.

We characterized our system on a centrifugal microfluidic "lab-on-a-disk" platform. Yet, this measurement setup may be readily deployed in pressure driven microfluidic systems as well. To this end, a channel pair as shown in Fig. 1 must be embedded in the microfluidic chip. Advancing towards real-world applications, we propose to use our system in centrifugal microfluidics for measuring viscosities of liquid samples. Furthermore, in pressure driven microfluidic platforms, our system could be beneficial to detect the presence of (usually) unwanted air bubbles. By real-time monitoring of liquid levels and flow rates, the reproducibility of assays can be significantly improved. Additionally, the sensor principle may facilitate lab-on-a-chip applications like the on-line detection of sedimentation assays[33] or absorption assays.[34] Furthermore, data can be used technically for quality control, closed-loop flow control and calibration purposes.

References

1 D. Janasek, J. Franzke and A. Manz, *Nature*, 2006, **442**, 374–380.
2 L. Bocquet and E. Charlaix, *Chem. Soc. Rev.*, 2010, **39**, 1073–1095.
3 A. Manz, N. Graber and H. M. Widmer, *Sens. Actuators, B*, 1990, **1**, 244–248.
4 D. Mark, S. Haeberle, G. Roth, F. von Stetten and R. Zengerle, *Chem. Soc. Rev.*, 2010, **39**, 1153–1182.
5 A. Arora, G. Simone, G. B. Salieb-Beugelaar, J. T. Kim and A. Manz, *Anal. Chem.*, 2010, **82**, 4830–4847.
6 P. S. Dittrich and A. Manz, *Nat. Rev. Drug Discovery*, 2006, **5**, 210–218.
7 A. M. Skelley and J. Voldman, *Lab Chip*, 2008, **8**, 1733–1737.
8 C. C. Liu, J. A. Thompson and H. H. Bau, *Lab Chip*, 2011, **11**, 1688–1693.
9 K. A. Muirhead, P. K. Horan and G. Poste, *Bio/Technology*, 1985, **3**, 337–356.
10 D. A. Czaplewski, B. R. Ilic, M. Zalalutdinov, W. L. Olbricht, A. T. Zehnder, H. G. Craighead and T. A. Michalske, *J. Microelectromech. Syst.*, 2004, **13**, 576–585.
11 M. Ashauer, H. Glosch, F. Hedrich, N. Hey, H. Sandmaier and W. Lang, *Sens. Actuators, A*, 1999, **73**, 7–13.
12 J. Chen, Z. F. Fan, J. Zou, J. Engel and C. Liu, *Journal of Aerospace Engineering*, 2003, **16**, 85–97.
13 A. Glaninger, A. Jachimowicz, F. Kohl, R. Chabicovsky and G. Urban, *Sens. Actuators, A*, 2000, **85**, 139–146.
14 S. Y. Wu, Q. Lin, Y. Yuen and Y. C. Tai, *Sens. Actuators, A*, 2001, **89**, 152–158.
15 Y. C. Tung, M. Zhang, C. T. Lin, K. Kurabayashi and S. J. Skerlos, *Sens. Actuators, B*, 2004, **98**, 356–367.
16 J. A. Wu and W. Sansen, *Sens. Actuators, A*, 2002, **97–8**, 68–74.
17 R. E. Oosterbroek, T. S. J. Lammerink, J. W. Berenschot, G. J. M. Krijnen, M. C. Elwenspoek and A. van den Berg, *Sens. Actuators, A*, 1999, **77**, 167–177.
18 J. Collins and A. P. Lee, *Lab Chip*, 2004, **4**, 7–10.
19 Z. F. Fan, J. Chen, J. Zou, D. Bullen, C. Liu and F. Delcomyn, *J. Micromech. Microeng.*, 2002, **12**, 655–661.
20 G. J. M. Krijnen, M. Dijkstra, J. J. van Baar, S. S. Shankar, W. J. Kuipers, R. J. H. de Boer, D. Altpeter, T. S. J. Lammerink and R. Wiegerink, *Nanotechnology*, 2006, **17**, S84–S89.
21 A. Quist, A. Chand, S. Ramachandran, D. Cohen and R. Lal, *Lab Chip*, 2006, **6**, 1450–1454.
22 F. Bundgaard, O. Geschke, R. Zengerle and J. Ducrée, A simple opto-fluidic switch detecting liquid filling in polymer-based microfluidic systems, *Proceedings of the 14th International Conference on Solid-State Sensors, Actuators and Microsystems (Transducers & Eurosensors '07)*, Lyon, France, 2007; pp. 759–762.

23 J. Ducrée, S. Haeberle, S. Lutz, S. Pausch, F. von Stetten and R. Zengerle, *J. Micromech. Microeng.*, 2007, **17**, S103–S115.
24 R. Gorkin, J. Park, J. Siegrist, M. Amasia, B. S. Lee, J. M. Park, J. Kim, H. Kim, M. Madou and Y. K. Cho, *Lab Chip*, 2010, **10**, 1758–1773.
25 B. S. Lee, U. L. Yang, H.-S. Kim, T.-H. KIm, J. Park, J.-G. Lee, J. KIm, H. Kim, W. G. Lee and Y. K. Cho, *Lab Chip*, 2011, **11**, 70–78.
26 M. C. R. Kong and E. D. Salin, *Anal. Chem.*, 2010, **82**, 8039–8041.
27 D. A. Duford, D. D. Peng and E. D. Salin, *Anal. Chem.*, 2009, **81**, 4581–4584.
28 K. bi-Samra, R. Hanson, M. Madou and R. A. Gorkin, *Lab Chip*, 2011, **11**, 723–726.
29 M. Grumann, T. Brenner, C. Beer, R. Zengerle and J. Ducrée, *Rev. Sci. Instrum.*, 2005, **76**, 025101–025106.
30 J. Ducrée, habilitation treatise, *IMTEK - University of Freiburg*, 2005.
31 Y. Y. Hou and H. O. Kassim, *Rev. Sci. Instrum.*, **2005**, 76.
32 C. W. Macosko, in *Rheology: Principles, measurements, and applications*, VHC, New York, 1994.
33 L. Riegger, M. Grumann, J. Steigert, S. Lutz, C. P. Steinert, C. Mueller, J. Viertel, O. Prucker, J. Ruhe, R. Zengerle and J. Ducree, *Biomed. Microdevices*, 2007, **9**, 795–799.
34 J. Steigert, M. Grumann, T. Brenner, L. Riegger, J. Harter, R. Zengerle and J. Ducrée, *Lab Chip*, 2006, **6**, 1040–1044.

